

**Thermal behavior and operating requirements
of IFE direct-drive target**

A. R. Raffray, J. Pulsifer, M. S. Tillack and X. Wang

November 15, 2002



**Fusion Division
Center for Energy Research**

University of California, San Diego
La Jolla, CA 92093-0417

THERMAL BEHAVIOR AND OPERATING REQUIREMENTS OF IFE DIRECT-DRIVE TARGET

A. R. Raffray¹, J. Pulsifer³, M. S. Tillack¹, and X. Wang³

¹Mechanical and Aerospace Engineering Department and Center for Energy Research, University of California, San Diego, EBU-II, Room 460, La Jolla, CA 92093-0417

³Center for Energy Research, University of California, San Diego, EBU-II, Room 460, La Jolla, CA 92093-0417

**Technical Report
UCSD-ENG-097
November 15, 2002**

ABSTRACT

During injection, inertial fusion energy (IFE) direct drive targets are subject to heating from energy exchange with the background gas and radiation from the wall. This heat deposition could lead to deuterium-tritium (DT) phase change and target deformation violating the target physics symmetry requirements. This paper assesses the thermal behavior of the target under such conditions and explores possible ways of extending the target lifetime through design modification(s) and/or through a better understanding of the effect of energy deposition and phase change on the target density symmetry.

I. INTRODUCTION

A typical inertial fusion energy direct drive target consists of a spherical shell (~4 mm in diameter) composed mainly of solid DT at 18K, as illustrated in Fig. 1. It is injected at velocities up to about 400 m/s in an IFE chamber. Once the target reaches the center of the chamber, the driver is fired, focusing energy on the target to create the fusion micro-explosion. To obtain the maximum energy yield from the fusion reaction, the temperature of the frozen DT layer must be held at about 18.5 K and the target must maintain a high degree of spherical symmetry and surface smoothness when it reaches the center of the chamber.

During injection, the target is subject to heating from energy exchange with the background gas as well as from radiation from the chamber walls. The resulting target thermal

behavior is a particular concern because the target can deform due to melting and evaporation of the DT. Deformation of the outer layer of target material can greatly affect the target gain and possibly prevent the target from properly functioning. Although the maximum temperature limit to prevent unacceptable target outer layer deformation is not well known, the previous assumption was to maintain the target surface temperature below the triple point of DT (19.79 K) [1].

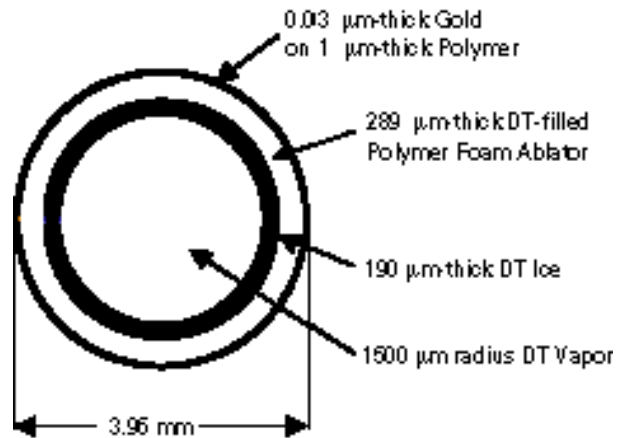


Figure 1 Example direct-drive target configuration [1]

This report presents an updated and more detailed assessment of the target thermal behavior during injection. The heating threats are first characterized. The initial thermal analyses based on maintaining DT below its triple point are then summarized. Next, possible ways of increasing the target design operating windows are investigated in a two-prong fashion: (1) enhancing the target thermal robustness through design modifications; and (2) exploring the possibility of extending the DT thermal limit by better understanding the effect of energy deposition and phase change on the target density symmetry relative to target physics requirements. For this purpose, a simple semi-integrated thermo-mechanical model has been derived to provide supporting analyses. Finally, conclusions are provided including recommended directions for future R&D effort.

II. TARGET HEATING

An important component of the heat transfer to the target is associated with the transfer of energy from the impinging background gas

(such as xenon or helium) which might be needed in the chamber for wall protection and through which the target must travel. Such heating processes would include “convection” as well as condensation if the background gas boiling and melting points are higher than the target temperature (e.g. for Xe). In addition, if plasma conditions remain in the chamber, recombination of ions at the surface would result in even larger heat transfer. Much uncertainty remains regarding plasma conditions during injection which is currently being investigated. For simplicity, plasma effects are not included in the calculations presented here with the understanding that the results would have to be revisited as new information on plasma remnants in the chamber becomes available.

Convection heat transfer from the background gas to the target has been analyzed previously over different regimes (molecular, transition and continuum) but without explicitly considering condensation [2]. For the 4-mm target case, the transition regime (Knudsen number $\sim 0.1-10$) applies for Xe pressure of about 100 mtorr (at 300 K) or lower and the full molecular regime for Xe pressure of ~ 1 mtorr (at 300 K) or lower. These include the range of pressures anticipated for a direct drive target with a dry wall; clearly continuum regime convection heat transfer would not apply. For this reason, a direct simulation Monte Carlo (DSMC) program was used to determine the heat flux at the surface of an IFE target [3]. The DSMC computations of the heat flux assume that the temperature of the impinging Xe atoms drops to 18 K, but that no Xe atoms stick to the target surface. Rather, they drop in temperature and then reflect from the surface where they provide a shield against subsequent atom collisions. However, depending on the condensation coefficient, a significant fraction of Xe atoms could stick to the target surface thereby not shielding subsequent atom collisions and resulting in higher, more challenging heat fluxes on the target. A condensation analysis was done to assess this possibility [3].

Figure 2 illustrates the results in term of the maximum condensation heat flux as a function of the product of Xe pressure and condensation

coefficient ($\bar{\alpha}_c P_{Xe}$) for cases with different Xe temperatures and injection velocities. These results for q''_{max} were found to be consistent with those from DSMC runs for condensation coefficients, $\bar{\alpha}_c$'s, ranging from ~ 0.5 at 100 mtorr to ~ 1 at 1 mtorr. The range in $\bar{\alpha}_c$ values can be explained from the assumptions used in DSMC where, for very low pressure, shielding of subsequent atom collisions by atoms reflecting from the surface would be minimal (with $\bar{\alpha}_c = 1$ from the corresponding condensation analysis) whereas shielding is more effective as the Xe pressure increases (with correspondingly lower $\bar{\alpha}_c$'s from the condensation analysis). No data were found for the condensation coefficient for Xe at $\sim 1,000$'s K condensing on an 18 K surface since no data were found for this specific case. However, experimental data from Ref. [4] indicate $\bar{\alpha}_c$ values of 0.99-0.6 for 2,500 K Ar beam condensing on an 15 K Cu/Ar with incident angle of $0^\circ-60^\circ$. Thus, it seems prudent to assume $\bar{\alpha}_c$ values of ~ 1 to estimate condensation heat fluxes

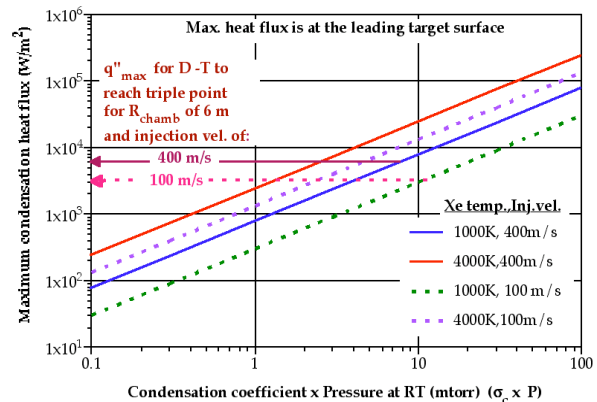


Figure 2. Maximum condensation heat flux as a function of the product of accommodation coefficient and Xe pressure at 300 K ($\bar{\alpha}_c P_{Xe}$) for cases with different Xe temperatures and injection velocities.

Results for convection heat flux from a He background gas were found to be somewhat higher than those from the Xe case even in the absence of condensation. This can be explained as follows: (1) the latent heats have only a small effect on the overall energy transfer which is mostly governed by the change in the gas enthalpy; and (2) the molecular flux of He on the moving target are higher than those of Xe for the same pressure and temperature [3].

However, use of He has the advantage that the He atoms after transferring their energy to the 18 K target will likely be reflected back thereby shielding the target from subsequent He atom collisions.

A simple estimate of the radiation heat flux, q_{rad} on the target during injection is given by:

$$q_{rad}'' = (1 - \epsilon) \sigma_{S-B} T_w^4 \quad (1)$$

where T_w is the wall temperature (assumed as a black body), σ_{S-B} is Stefan-Boltzmann constant, and ϵ the target surface reflectivity. A very reflective target surface is required to minimize the total absorbed heat flux. For the very thin (275–375 Å) coating of gold on the target, a reflectivity of about 96% is anticipated [1]. An effort is underway to estimate more accurately the radiated energy absorption and reflection based on a multi-layer wave model to provide a stronger basis for this assumed reflectivity. As an illustration, q_{rad}'' from eq. (1) ranges from 2300 W/m² for $T_w=1000$ K to 11,000 W/m² for $T_w=1500$ K.

III. TARGET THERMAL ANALYSIS

The thermal response of the target (shown in Fig. 1) to incident heat flux was determined parametrically assuming a 2-D heat flux distribution over the target similar to those from the DSMC results[3]. The ANSYS finite element code[5] was used for this transient thermal analysis which assumed that the target is not tumbling (i.e. the same side of the target is always facing forward and the leading edge of the target is exposed to the maximum heat flux during the entire time of flight). Temperature dependent DT properties were used including the latent heat of fusion at the triple point to model the phase change [3].

Figure 3 summarizes the results for a target injected at 400 m/s in the chamber. It shows the maximum temperature change of the target as a function of the maximum heat flux at the target surface for 3 different chamber radii (affecting the time of flight for a given injection velocity). The temperature change of the target increases in a linear fashion up to the triple point of DT. At the triple point, there is a knee in the curve where additional heat flux does not affect the temperature as much, consistent with the

phase change when going from solid to liquid DT. From the figure, the heat flux to reach the triple point is about 6000 W/m² for a 6-m radius chamber and even lower for larger chambers. From Fig. 2, this corresponds to a condensation heat flux from Xe at 1000K and 7.6 mtorr or at 4000 K and 2.5 mtorr (for $\epsilon_c=1$); and from eq. (1) to a radiation heat flux from a wall at 1275 K. This would place an important constraint on background gas density that might be required for wall protection.

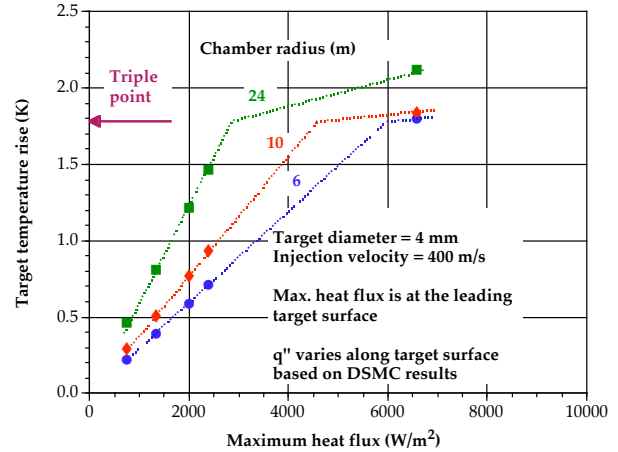


Figure 3. Target DT temperature change as a function of incident heat flux

IV. TARGET DESIGN MODIFICATION TO ENHANCE THERMAL ROBUSTNESS

One of the measures envisaged to enhance the thermal robustness of the target is the inclusion of a porous plastic foam layer on the outside of the target to provide thermal insulation that would delay the heat transfer to the DT region of the target and help extend its lifetime during injection. One assumption is to replace some of the DT-foam region by this outer (and empty) porous foam layer subject to confirmation from target physics requirements [6].

The temperature properties of the cryogenic foam were based on those of fully dense polystyrene. The density was adjusted based on the assumed porosity of the foam region. For simplicity, the thermal conductivity of the porous foam was similarly adjusted and then further scaled by a factor of 2/3 to account for possible optimization of the porous microstructure to minimize the conductivity. As a conservative measure, the higher thermal conductivity values found in the literature were

used in this study consistent with those used by Siegel [2], with values ranging from 0.088 W/m-K at 19 K to 0.13 W/m-K at 40 K. The heat capacity values used range from 100 J/kg-K at 20 K to 2225 J/kg-K at 40 K[6].

The transient analyses were performed using ANSYS and the results are illustrated in Figure 4 for a maximum incident heat flux of 2.2 W/cm² (e.g. corresponding to condensation of 10 mTorr, 4000 K Xe from Fig. 2). The figure shows the DT interface temperature history during injection for a target with a 25% dense outer foam layer of various thicknesses. In this case a thickness of about 130 microns (32 microns of equivalent solid polystyrene) would be sufficient to prevent the DT interface temperature from reaching the triple point after 0.015 s (corresponding to a target velocity of 400 m/s in a chamber of radius 5 m). As comparison the DT interface temperature would reach the triple point after about 0.0022 s in the absence of the outer foam layer.

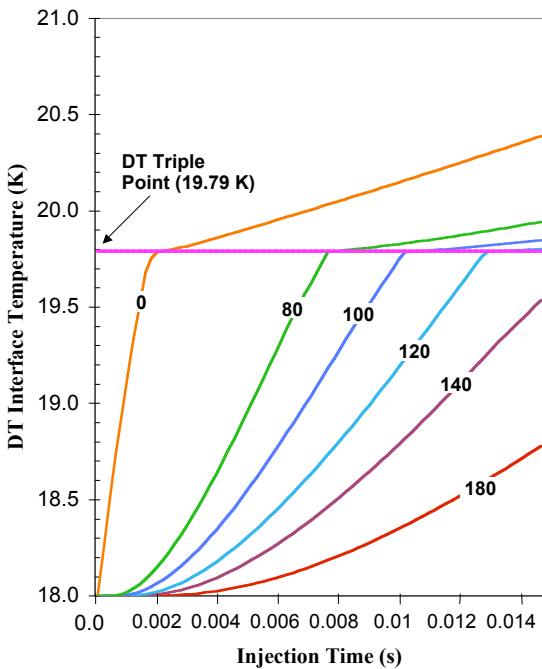


Figure 4 DT interface temperature history for various thicknesses (shown in microns on the lines) of a 25% dense outer foam insulating layer under an incident heat flux of 2.2 W/cm².

The results also showed that the time for DT to reach the triple point is increasingly retarded as the foam density is decreased due in good part to the large increase in heat capacity as the temperature of the foam increases. For example, for a 100- μ m outer foam region the time for DT to reach its triple point increases from \sim 0.106 s to \sim 0.126 s as the foam density is reduced from 25% to 10%. Thus, for increased target thermal robustness, it is preferable to maximize both the thickness and porosity of the outer foam layer to values that can still accommodate the target physics and structural integrity requirements. For example, a 152 μ m-thick 10% dense insulating foam layer would accommodate a heat flux of up to 7.5 W/cm² (e.g. corresponding to condensation from 1000K, 100mTorr Xe) while maintaining DT below its triple point after up to \sim 0.015 s of flight time.

The possibility of increasing the plastic coating thickness from \sim 1 μ m to 10 μ m to provide added insulation was also assessed but was found to provide only marginal improvement.

V. THERMO-MECHANICAL ANALYSIS

Another means to extend the target lifetime is by relaxing the DT thermal limit through a better understanding of the effect of energy deposition and phase change on the target density symmetry relative to target physics requirements. From Fig. 1, the target is covered by a \sim 1 μ m solid plastic coating. Under heating, the concern is that vapor might form at the DT-foam/plastic coating interface resulting in unacceptable density variation for proper target functioning. If the bond between DT-foam and the plastic coating is perfect, vapor formation will only occur through homogeneous nucleation. However, under target conditions, homogeneous nucleation is virtually zero at temperatures lower than 26 K and dramatically increases as the temperature approaches 34 K. Heterogeneous nucleation could be a problem but assumes the presence of nucleation sites of the order of 1 μ m. This presupposes some imperfection in the DT-foam/plastic coating bond. Such imperfection could also lead to a micro-gap at the interface which would favor surface evaporation. This scenario was further assessed.

It was assumed that as heat reaches the DT-foam/plastic coating interface during injection, the DT temperature increases to the triple point (19.79 K) and DT starts to melt and to vaporize. The pressure build-up due to phase change (both DT liquid and vapor have lower densities than solid DT) must be counterbalanced by the stress in the plastic coating which provides the structural element. A simple semi-integrated thermo-mechanical model was derived for the analysis.

The model is based on a spherical target (shown schematically in Figure 5) with the DT-foam/plastic coating at a radius, R_{int} and a plastic coating of thickness, $t_{plastic}$. A thickness, d_{p-c} , of the DT interface undergoes phase change, most of which will be in liquid form but there might be some vapor depending on the local pressure and temperature. Let us assume that a mass fraction x_l of the phase change is liquid and $(1-x_l)$ is vapor.

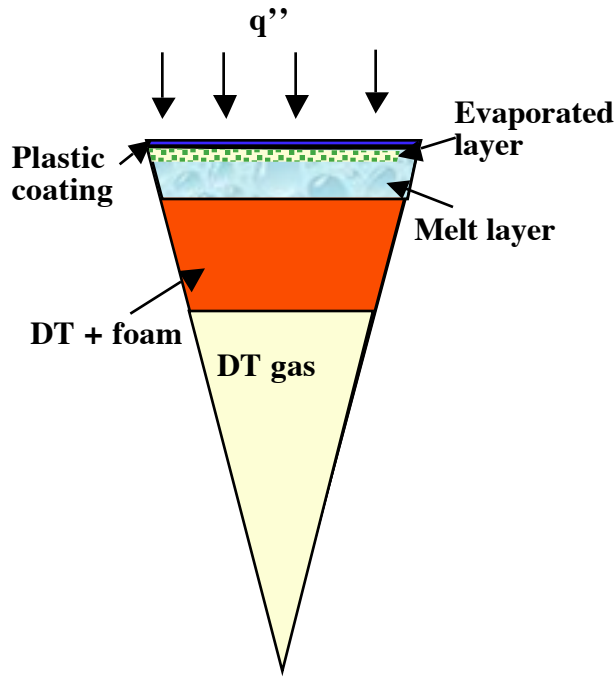


Figure 5 Schematic of target showing DT undergoing phase change

The initial solid volume, V_s , that has undergone phase change is given by:

$$V_s = \frac{4}{3} \pi (R_{int}^3 - (R_{int} - d_{p-c})^3) \quad (2)$$

The volume of liquid, V_l , within the phase change mass is:

$$V_l = V_s \frac{\rho_s}{\rho_l} x_l \quad (3)$$

where ρ_s and ρ_l are the DT solid and liquid densities, respectively. The volume of vapor, V_v , is given by:

$$V_v = V_s \rho_s (1 - x_l) R_{DT} \frac{T_v}{P} \quad (4)$$

where R_{DT} is the DT vapor gas constant (1663 J/kg-K), T_v is the vapor temperature and P the pressure. The change in volume, ΔV , is then given by:

$$\Delta V = V_l + V_v - V_s \quad (5)$$

The plastic coating will also undergo a change in volume, ΔV_{th} due to thermal expansion:

$$\Delta V_{th} = \frac{4}{3} \pi R_{int}^3 ((1 + \alpha \Delta T_{pl})^3 - 1) \quad (6)$$

where α is the plastic coefficient of thermal expansion and ΔT_{pl} is the plastic temperature rise.

If $\Delta V > \Delta V_{th}$, the plastic coating will undergo a volumetric strain which can be equated to an internal pressure P , given by: [7]

$$\frac{\Delta V - \Delta V_{th}}{V_{target}} = \frac{6PR_{int}}{4t_{plastic}E} (1 - \nu) \quad (7)$$

where E and ν are the plastic coating Young's modulus and Poisson's ratio, respectively.

Substituting for ΔV from eq. (5), and for V_l and V_v from eqs. (3) and (4) yields:

$$\left(\frac{x_l \rho_s}{\rho_l} + \frac{(1 - x_l) \rho_s R_{DT} T_v}{P} - 1 \right) V_s - \Delta V_{th} = V_{target} \frac{6PR_{int}}{4t_{plastic}E} (1 - \nu) \quad (8)$$

If all other parameters are known, eq.(8) represents a quadratic equation which can be solved for P .

The resulting hoop stress, σ_h , on the plastic coating can then be calculated as [7]:

$$\delta_h = \frac{PR_{int}}{2t_{plastic}} \quad (9)$$

All parameters required for the solution of eq. (9) are known except for the temperature, the phase change thickness and the mass fraction of liquid in the phase change mix. From an ANSYS thermal analysis of the DT interface including melting at the triple point, the maximum temperature of DT and the corresponding melt thickness can be estimated for different heat fluxes assuming a 0.015 s flight time. The results are summarized in Figs. 6 and 7. Since it is assumed that most of the phase change will actually consist of liquid, it seems reasonable to assume that the melt layer obtained from the ANSYS calculations (under constant volume assumptions) represent the phase change thickness. Thus from curve fitting of Figs. 6 and 7, the incident heat flux (W/cm^2) and DT interface temperature (K) can be obtained as functions of the phase change thickness (μm).

$$T_{int} = 9.17e-5d_{p-c}^3 - 1.12e-3d_{p-c}^2 + 0.016d_{p-c} + 19.816 \quad (10)$$

$$q'' = 5.7e-6d_{p-c}^3 - 4.63e-4d_{p-c}^2 + 0.0623d_{p-c} + 0.662 \quad (11)$$

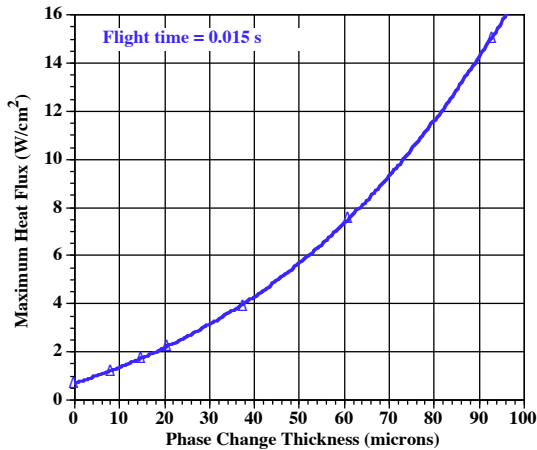


Figure 6 Combination of maximum heat flux and phase change thickness obtained from ANSYS analyses

Figure 8 shows the phase diagram for DT. To minimize the liquid pressure (and pressure on the plastic coating) for a given temperature, the liquid at the interface should be saturated (i.e. at the point along the evaporation P-T line

on the phase diagram corresponding to the liquid temperature). Curve fitting the DT saturation line yields the following expression for the interface temperature as a function of pressure:

$$T_{int} = 5.2911 P^{0.1356} \quad (12)$$

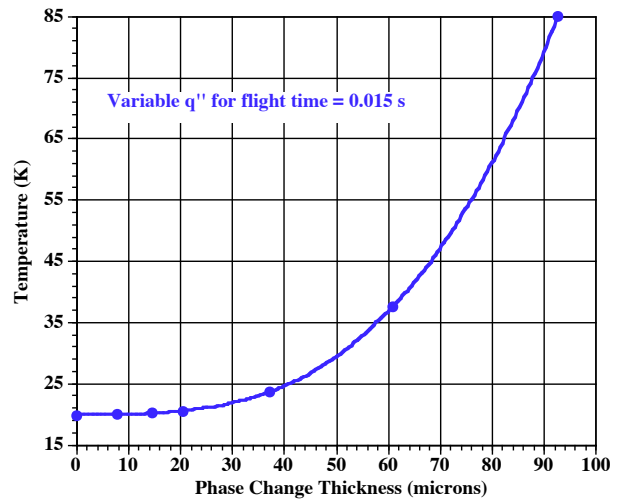


Figure 7 Combination of interface temperature and phase change thickness obtained from ANSYS analyses

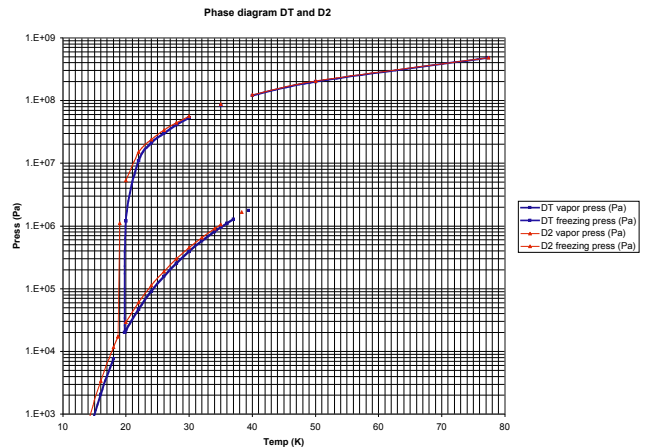


Figure 8 DT phase diagram

If there is vapor formed the vapor could be at a higher temperature but still at the same pressure as the liquid. The temperature rise through the vapor can be estimated from the heat flux, the thickness of the vapor region and the thermal conductivity of the vapor. At the same time the combination of vapor temperature

and specific volume must be such as to maintain the same pressure as that of the liquid at the saturation point.

The analysis was done for different phase change thicknesses (i.e incident heat flux) and the results are summarized in Figures 9-11. Figure 9 shows the vapor region thickness as a function of the maximum incident heat flux for different plastic coating thicknesses. Figure 10 shows the temperature as a function of the heat flux. The vapor region thickness is lower for thicker plastic coating. For an 8- μm thick coating, the evaporated layer thickness is $<2.5 \mu\text{m}$ for heat fluxes $<4 \text{ W/cm}^2$.

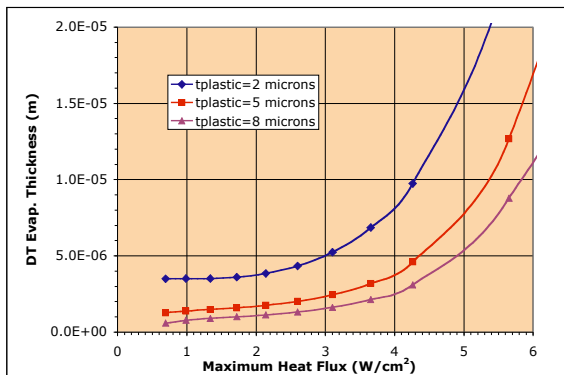


Figure 9 Vapor region thickness as a function of the maximum incident heat flux for different plastic coating thicknesses.

Figure 10 shows the hoop stress in the plastic coating as a function of the heat flux for different plastic coating thicknesses. Also shown is the equivalent pressure in the DT liquid and vapor regions. The ultimate tensile strength of polystyrene is $\sim 30\text{-}60 \text{ MPa}$. Based on the lower value, the maximum allowable heat flux ranges from 4 to 5.5 W/cm^2 for plastic coating thicknesses of 2 to $8 \mu\text{m}$, respectively.

Allowing for vapor formation would relieve the demand on design modifications such as adding an insulating foam layer for reasonable heat flux accommodation. Example results for a case with a $72 \mu\text{m}$ 25% dense outer foam layer are summarized in Figures 12 to 14. From Fig. 12, the allowable incident flux to maintain an evaporation layer thickness $\sim 3 \mu\text{m}$ is $\sim 9 \text{ W/cm}^2$ for a plastic coating thickness of $8 \mu\text{m}$. This thickness corresponds to about a 1% density

variation for the $289 \mu\text{m}$ DT/foam region. The corresponding hoop stress is $< 30 \text{ MPa}$ as shown in Figure 13.

Figure 11 shows the average vapor temperature as a function of the heat flux for the different plastic coating thicknesses. Also shown is the vapor/liquid interface temperature.

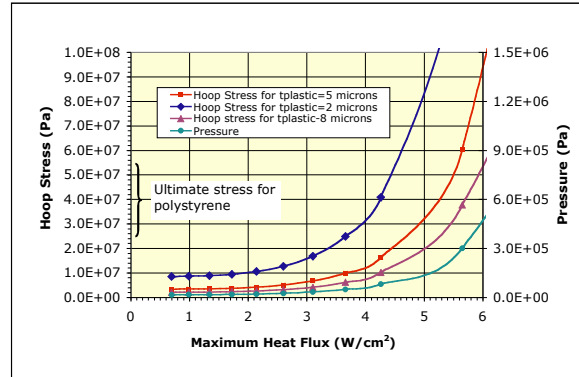


Figure 10 Hoop stress in the plastic coating as a function of the heat flux for different plastic coating thicknesses. Also shown is the equivalent pressure in the DT liquid and vapor regions.

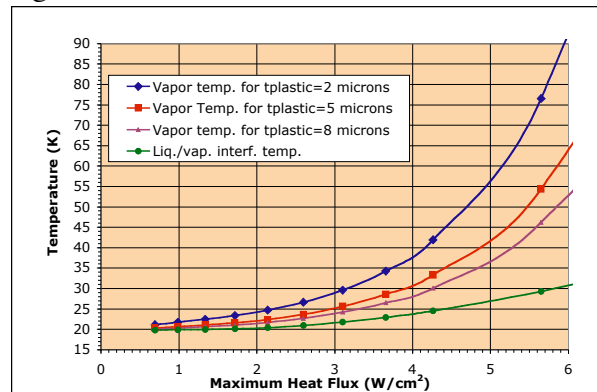


Figure 11 Average vapor temperature as a function of the heat flux for the different plastic coating thicknesses. Also shown is the vapor/liquid interface temperature.

The results from this simple thermo-mechanical model have helped to highlight the benefits of relaxing the DT vapor formation constraint and of including design modifications such as an insulating outer layer. However, this model has limitations. It does not include the latent heat of vaporization which can affect the vapor conditions. It also assumed a rigid DT ice inner boundary. Any deformation of this boundary would relieve the

pressure and affect vapor formation. It also can be cumbersome relying on curve fitting of ANSYS results to provide the necessary relations between heat flux, interface temperature and phase change thickness. A fully integrated model including the interactions of all key processes would be a very useful tool to further understand the phase change process and its effect on the target symmetry. Such an integrated model would include a better boiling model, integration of thermal and mechanical processes and would calculate the transient thermo-mechanical and phase change behavior in a consistent way.

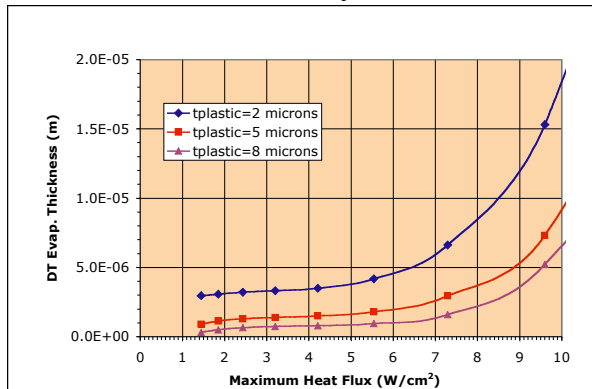


Figure 12 Vapor region thickness as a function of the maximum incident heat flux for different plastic coating thicknesses for a case with a 72 μm 25% dense outer foam layer.

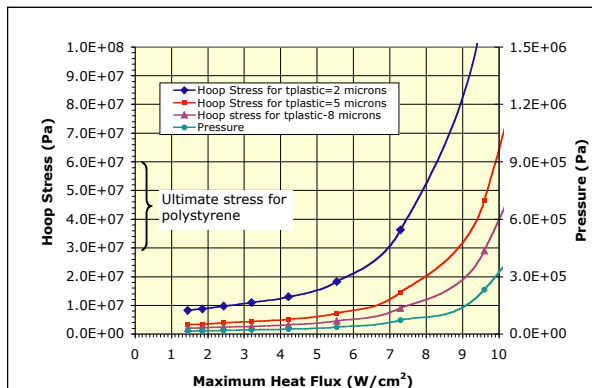


Figure 13 Hoop stress in the plastic coating as a function of the heat flux for different plastic coating thicknesses for a case with a 72 μm 25% dense outer foam layer. Also shown is the equivalent pressure in the DT liquid and vapor regions.

VI. CONCLUSIONS

The potential benefit on target lifetime of adding an insulating foam layer and/or of better

understanding vapor formation processes have been examined. For the typical target configuration shown in Fig. 1, the maximum q_{inc}'' for DT to reach its triple point is only about 0.6 W/cm² for a 6-m radius chamber and even lower for larger chambers. This would place an important constraint on background gas density that might be required for wall protection. Adding an insulating outer foam layer on the target helps to increase the target lifetime. Adding a 130- μm 25% dense outer foam layer would increase the allowable q_{inc}'' for DT to reach its triple point to 2.2 W/cm² and a 152- μm 10% dense insulating foam layer would accommodate a heat flux of up to 7.5 W/cm². For increased target thermal robustness, it is preferable to have the maximum thickness and porosity outer foam layer which can still accommodate the target physics and structural integrity requirements.

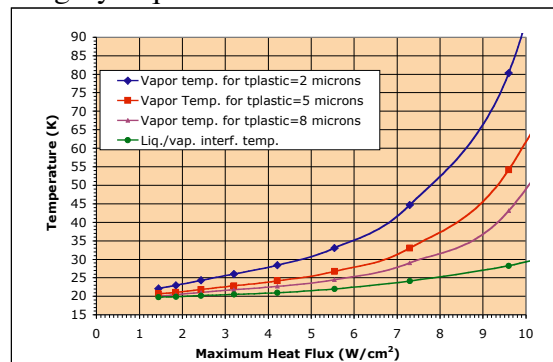


Figure 14 Average vapor temperature as a function of the heat flux for the different plastic coating thicknesses for a case with a 72 μm 25% dense outer foam layer. Also shown is the vapor/liquid interface temperature.

Allowing for vapor formation would relieve the demand on design modifications such as adding an insulating foam layer for reasonable heat flux accommodation. A simple thermo-mechanical model was developed to help in better understanding the DT phase change process. A thicker plastic coating was found preferable to reduce the vapor region thickness. If it were assumed that $\sim 1\%$ change in region density was acceptable based on target physics requirements, $\sim 3\mu\text{m}$ of vapor region at the DT-foam/plastic coating interface would be acceptable. Under these conditions, the maximum allowable q_{inc}'' is ~ 4 W/cm² for the original target design and up to 9 W/cm² for a

target design with 72- μ m thick, 25%-dense outer insulating foam layer and an 8- μ m thick plastic coating. In both cases, the corresponding hoop stresses in the plastic coating are less than the anticipated ultimate tensile strength.

The results from the simple thermo-mechanical model have helped to highlight the benefits of relaxing the DT vapor formation constraint and of including design modifications such as an insulating outer layer. However, this model has limitations and a better understanding of the phase change processes would be obtained from a fully integrated model including the interactions of all key processes. For example, the assumption of surface evaporation is conservative and assumed the presence of a minute gap at the DT-foam and plastic coating interface; for a good-quality interface bond, DT boiling is more likely to occur through nucleation which should be included in the model. This also indicates the need for an experimental effort to better characterize the quality and behavior of this bond ideally by using or possibly by simulating the actual materials. In addition, guidance is needed from the target physics perspective to understand better the constraints and limitations imposed on such actions.

ACKNOWLEDGEMENT

This work was supported by a Contract from General Atomics.

REFERENCES

1. R.W. Petzoldt, et al., "Direct Drive Target Survival During Injection in an Inertial Fusion Energy Power Plant," submitted to Nuclear Fusion, August 2002.
2. N. P. Siegel, "Thermal Analysis of Inertial Fusion Energy Targets," Master of Science Thesis, San Diego State University, May 2000.
3. A. R. Raffray, M. S. Tillack and J. Pulsifer, "Target Thermal Response and Gas Interactions," Fusion Program Technical Report, UCSD-ENG-092, June 2002
4. R. F. Brown, D. M. Trayer, and M. R. Busby, "Condensation of 300-2500 K Gases on Surfaces at Cryogenic Temperatures," The Journal of Vacuum Science and Technology, Vol. 7, No. 1, 1969.
5. ANSYS 5.7, ANSYS Inc., Canonsburg, PA
6. A. R. Raffray, J. Pulsifer, M. S. Tillack and X. Wang, "Effect of Outer Insulating Porous Plastic Foam Layer on Target Thermal Response During Injection," Fusion Program Technical Report, UCSD-ENG-096, October 2002
7. S. A. Urry, "Solution of Problems in Strength of Materials," Second Edition, Pitman paperbacks, Bath, Great Britain, 1971.